



Full length article

Mesoscale modeling of jet initiation behavior and microstructural evolution during cold spray single particle impact



Sumit Suresh^a, Seok-Woo Lee^a, Mark Aindow^a, Harold D. Brody^a, Victor K. Champagne^b, Avinash M. Dongare^{a,*}

^a Department of Materials Science and Engineering, Institute of Materials Science, University of Connecticut, 97 North Eagleville Road, Storrs, CT 06269, USA

^b Cold Spray Innovations International, Dudley, MA 01571, USA

ARTICLE INFO

Article history:

Received 9 July 2019

Revised 15 October 2019

Accepted 18 October 2019

Available online 25 October 2019

Keywords:

Cold spray

Particle impact

Jetting

Mesoscale

Molecular dynamics

Recrystallization

ABSTRACT

Quasi-coarse-grained dynamics (QCGD) simulations are carried out to investigate the mesoscale deformation behavior during the impact of a 20 μm pure aluminum particle onto a substrate of pure aluminum at time and length scales relevant to cold spray deposition. A rigorous analysis of the evolution of pressure, temperature, strain, flow stress and microstructure is carried out to investigate the jetting mechanisms over a range of process parameters (impact velocity and particle temperature). The QCGD simulations identify a critical role of the pressure wave propagation in the initiation of a jet, i.e. outward flow of material at the particle/substrate interface periphery (edge). Jetting is observed to initiate when the shock wave interacts with the edge and results in localized softening of the metal in this region. This localized softening enables outward flow of the material and is accompanied by a release of the pressures in the particle and the substrate at the interface. Observations of final splat microstructures of systems that showed jetting revealed several new “small” grains in the range of 2–4 μm. These grains are mainly found at the interface, suggesting that recrystallization is favored in cold sprayed impacts of aluminum.

© 2019 Acta Materialia Inc. Published by Elsevier Ltd. All rights reserved.

1. Introduction

Cold spray (CS) has recently emerged as a leading kinetic spraying technique for additive manufacturing and repair of metallic systems [1–7]. The process involves accelerating metal powders onto a substrate, which results in high strain rate deformation of the particles and bonding with the substrate [8]. CS has been successfully employed for a variety of metallic systems, from light-weight aluminum alloys [9–12] to heavy metals like tantalum [13]. The optimization of CS for desired applications necessitates a fundamental understanding of the complexities associated with particle impacts. Single particle impact studies can identify the particle/substrate adhesion and can be categorized depending on the nature of the material systems [14]. In situ monitoring of the particle/substrate deformation in experiments is currently obscured by physical constraints, and thus limited to observations of particle bonding or rebounding [15,16]. The characterization of the bonded particles (splats) reveal a jet-shaped material ejection (“jetting”) at the periphery of the particle/substrate interface. It is understood that jetting removes surface oxides and thus allows

a pristine metal-metal contact at the interface. Nevertheless, a recent study showed that even gold, a metal with no native oxide layer, showed jetting during bonding [17]. The proposed bonding mechanisms in the literature for metallic systems include oxide rupture [18–20], metallurgical bonding [21], mechanical interlocking [22–24], diffusion [25], localized melting [26], shock mechanics [27,28] and adiabatic shear instability (ASI) [29–31].

Several computational studies based on finite element methods (FEM) have explored the mechanisms of bonding during cold spray impact [8,9,15,25,27–32]. These studies have converged in identifying the concept of a “critical” velocity that is necessary for adhesion of the particle onto a substrate. The bonding of the particle to the substrate has been attributed to jetting, and is correlated to either ASI [14,29,30] or pressure wave interactions [28]. ASI involves the formation of a high-temperature zone due to severe plastic deformation, which leads to thermal softening and a breakdown in the flow stress at the interface. Experimentally, adiabatic shear bands are observed to be preceded by the nucleation, multiplication and growth of discontinuous islands of dynamic recrystallization [33,34]. The time scale of this phenomena has been predicted to be around tens of nanoseconds (~30 ns) for aluminum [14,29]. In contrast, the mechanism of pressure wave propagation behavior is based on a hydrodynamic spall process that renders the formation of a jet at relatively short timescales (~ 4 ns) [27].

* Corresponding author.

E-mail address: dongare@uconn.edu (A.M. Dongare).

The predictive capabilities of these models are, however, affected by the approximations used (meshing, strain rate dependence etc.) in the constitutive relationships at the continuum scales [35–38].

High strain rate impact deformations often result in micromechanisms like the formation of twins, microbands and dynamic recrystallization [39,40]. Modeling the deformation behavior of particle and substrate at length (microns) and time scales (nanoseconds) of CS while retaining an atomistic/discretized description is critical to observe such microstructural features. Unfortunately, the system size and time scales restrictions make this task unfeasible for an all-atom classical molecular dynamics (MD) simulation. “Quasi-coarse-grained dynamics” (QCGD) [41] extends the capabilities of classical MD simulations to the mesoscales by using representative atoms (R-atom) to define the collective dynamics of several atoms (Supplementary Note S1, [41–45]). This method is able to investigate the mesoscale microstructural evolution during single particle impact [45] and can provide additional scientific insights to the CS modeling knowledge base which has mostly been restricted to studying the evolution of thermomechanical variables. The objective of this study is therefore to use QCGD simulations to investigate the mechanisms of jet initiation and critically analyze the evolution of microstructure during single particle impact of a 20 μm -sized Al powder on an Al substrate.

2. Quasi-coarse-grained dynamics simulations of single particle impact

The QCGD simulations discussed here model the impact of a 20 μm polycrystalline Al powder particle onto a polycrystalline Al substrate with an average grain size of 10 μm created using the Voronoi tessellation method [46] for both the particle and the substrate. These microstructures and system dimensions require a level of coarsening of 512, i.e., L512 scaling. Essentially, this scaling value in terms of representing a microstructure means that one coarse unit cell (in QCGD), in this case face-centered cubic (fcc) aluminum, represents 512 regular fcc unit cells (in MD) in each of the three (X, Y and Z) dimensions. More details about these scaling relationships and the capability to model the thermodynamic behavior, mechanical behavior and impact behavior of Al are included in the Supplemental Material (Note S1 and Note S6). The system consists of a 20 μm diameter particle and a substrate cube with an edge length of 50 μm resulting in a total of ~60 Million R-atoms, wherein the energetics of the R-atoms are defined using L512 scaling relationships for the embedded atom method (EAM) interatomic potential for pure aluminum [47]. Damping boundary conditions are implemented at the edges to absorb any incoming compressive waves generated during impact, which can have an effect on the evolution of microstructure. The impact direction for all cases was maintained to be in the Z direction, i.e. perpendicular to the surface of the substrate. More details of the simulation setup are provided in Supplementary note S2. The L512-scaling relationships are able to reproduce the MD-predicted equation of state (EOS), thermodynamic behavior and the shock pressures and the shock temperatures as obtained for a time step of 2 fs. Prior to impact, the substrate is equilibrated at room temperature for all cases, i.e. 300 K and the particle at a temperature of ~165 K. The L512-QCGD simulations are able to model the morphological evolution of the powder particles during deformation and the role of powder and substrate deformation that lead to an outward/upward flow of both the particle and the substrate i.e. jet formation during single particle impact at the experimental time and length scales [45].

The QCGD simulations are performed to investigate the role of pressure wave propagation, and the temporal evolution of shear strains and temperature on the mechanisms of jet formation at the particle/substrate interface for impact velocities ranging from

700 m/s to 1300 m/s. It should be noted that the current capabilities of QCGD simulations do not include an oxide surface layer on the particle and/or the substrate, and hence impact results in the formation of a metallurgical bond when the Al particle is in contact with the substrate. Bonding mechanisms for particles related to rupture of oxide layers cannot be modeled in the current framework of the QCGD simulations. Thus, the systems modeled here are “clean”, i.e. devoid of typical inherent inclusions in experimental systems like roughness, porosity or an oxide layer. Due to the absence of particle rebound in the QCGD simulations, a challenge here is to define a “critical velocity” of bonding for single particle impact. Instead, the QCGD framework uses the occurrence of outward flow of the material at the particle/substrate interface ejection or “jet” as the “jetting velocity”. As a separate note to the reader, it is not the goal of this article to accurately predict critical velocities for CS. Predictions of such nature can be off due to exclusion of certain experimental features mentioned above, coarsening effects and the interatomic potential; the jetting velocity in this case can be overpredicted by a certain amount [45].

3. Temporal evolution of pressure, strains and temperature during jet initiation

Recent continuum models [27] have suggested that initiation of jetting during single particle impact is a result of the pressure waves that propagate and interact with the edge of the particle/substrate interface. This jet formation is attributed to particle-material ejection at the periphery of the bond interface due to formation of a tensile zone resulting in a “spall” process, which arises due to tensile pressures generated at the periphery of the particle/substrate interface. The pressure wave interaction with the edge is proposed as a critical factor for jetting to occur rather than the process of shear localization, and ASI was proposed to be a consequence of jetting rather than the cause. This hydrodynamic pressure wave driven process is analogous to that observed in liquid particle impact, wherein jetting is observed when the shock wave velocity exceeds the particle/substrate edge velocity [48,49].

The QCGD simulations are, therefore, carried out to investigate the role of pressure wave propagation behavior as well as the formation of a thermal boost-up zone that results in ASI at the interface. The evolution of temperature is compared for particle impact velocities of 700 m/s and 1300 m/s that are above and below the jetting velocity in the QCGD framework, respectively. As mentioned previously, the jetting velocity here is the velocity at which outward flow of the material is observed at the particle/substrate interface. The impact of an Al particle results in the generation of a pressure wave that propagates into the particle and the substrate, resulting in particle and substrate deformation and heat generation. The variations in the impact behavior above and below the jetting velocity is attributed to the variations in the evolution of pressures, temperatures and strains during impact that render the formation of a jet at the interface. Comparative snapshots for microstructure that do and do not form a jet are shown in Fig. 1 for the two impact velocities. The color of the atoms corresponds to the total energy of each R-atom in the QCGD simulations.

The temporal evolution of pressure in a thin vertical section (See Supplemental Figure S2 (b)) through the center of the particle is plotted in Fig. 2 (a)–(c) for an impact velocity of 1300 m/s, where “jetting” is observed, and in Fig. 2 (d)–(f) for an impact velocity of 700 m/s, where no jetting is seen. The contour levels are chosen to provide a clear visual impression of the compressive shock wave interaction with the particle edge, if any, and its role in initiating a jet. Note that “jetting” is defined in this work as initiation of outward flow at the particle/substrate interface periphery, rather than as material ejecting/spallation. The impact generates a compressive wave with a high pressure of ~11 GPa being recorded for

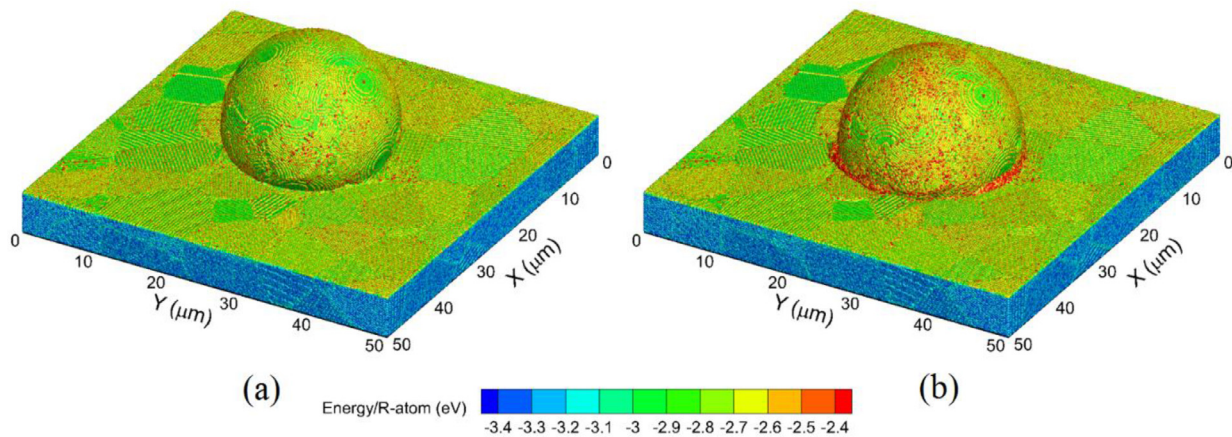


Fig. 1. Splat morphologies at different impact velocities: (a) 700 m/s (showing no jet) for the full duration of the simulation; and (b) 1300 m/s (showing jet initiation) for $T_p \sim 165$ K. The color of the atoms corresponds to the total energy of each R-atom in the QCGD simulations.

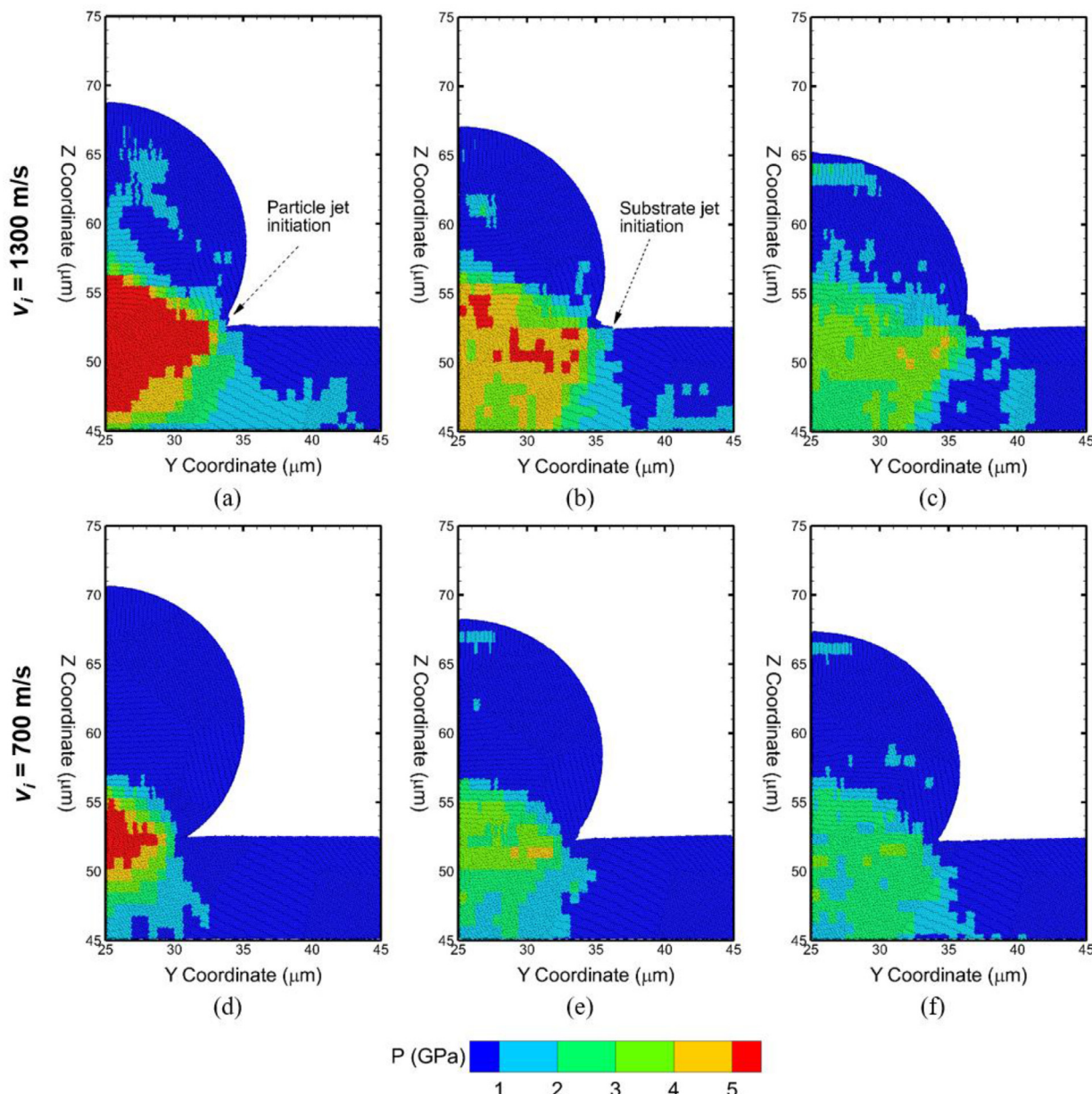


Fig. 2. Pressure evolution for $v_i = 1300$ m/s and $T_p \sim 165$ K at: (a) 2.9 ns, (b) 4.3 ns, and (c) 9.3 ns (after impact), and for $v_i = 700$ m/s and $T_p \sim 165$ K at: (d) 2.7 ns, (e) 6.7 ns, and (f) 10.3 ns (after impact). Pressure wave interaction with the interface is shown with the help of arrows.

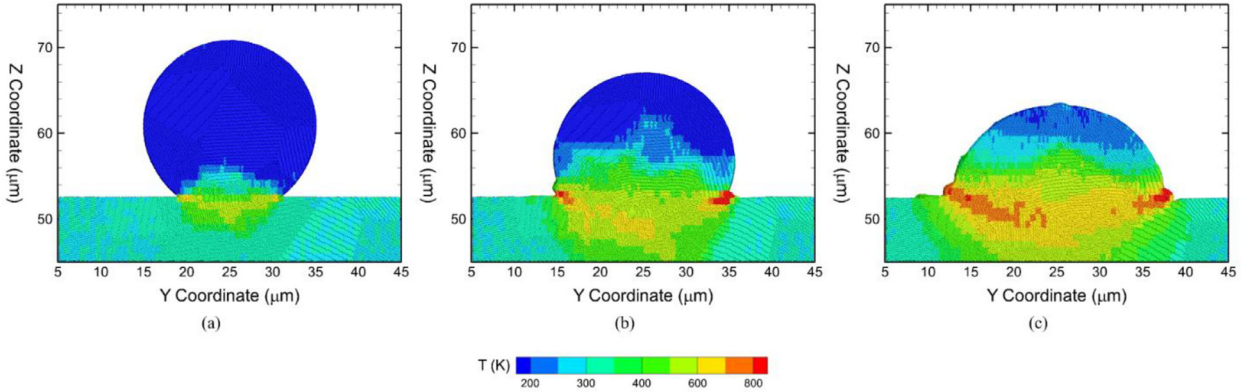


Fig. 3. Temperature evolution for the case of $v_i = 1300 \text{ m/s}$ and $T_p \sim 165 \text{ K}$ at: (a) 1.3 ns, (b) 4.3 ns, and (c) 9.3 ns (after impact).

an impact velocity of 1300 m/s in the region of impact. This compressive wave travels through the particle towards the back end, as well as along the particle/substrate interface, competing with the motion of the particle/substrate edge shear motion as shown in Fig. 2 (a)–(c). In this case the shock wave arrives the particle edge at $t = 2.9 \text{ ns}$ as shown in Fig. 2(a), that results in outward flow of the materials and a *particle jet* is initiated. The QCGD simulations predict that this wave interaction with the edge results in an outward flow of the material resulting in the formation of *substrate jet* at a time of 4.3 ns as shown in Fig. 2(b). This initiation of the jet results in a significant release/drop of the pressure in the particle and substrate at the interface as seen in Fig. 2(c). In this regard, previous continuum level studies have generally characterized jetting mechanisms only for the particle, whereas the QCGD simulations additionally demonstrate the role of the substrate in the formation of the jet. It should be noted that the QCGD simulations did not predict ejection/fragmentation of the material as observed in continuum simulations. In comparison, the 700 m/s impact generates a maximum compressive pressure of $\sim 8 \text{ GPa}$. The evolution of the pressure wave does not appear to interact with the particle/substrate interface edge, and no initiation of the jet is observed for the impact velocity of 700 m/s as shown in Fig. 2(d)–(f). Thus, jetting is only observed where the shock wave velocity along the particle/substrate interface exceeds the velocity of the edge during impact, as seen for the 1300 m/s single particle impact.

These observations demonstrate the critical role of the pressure wave evolution in the jetting behavior, and this is similar to the impact of a liquid particle [49] wherein a jet is observed only when the shock wave velocity along the interface exceeds the edge velocity. In contrast, the continuum modeling literature suggests that jetting initiation is attributed to ASI, wherein local

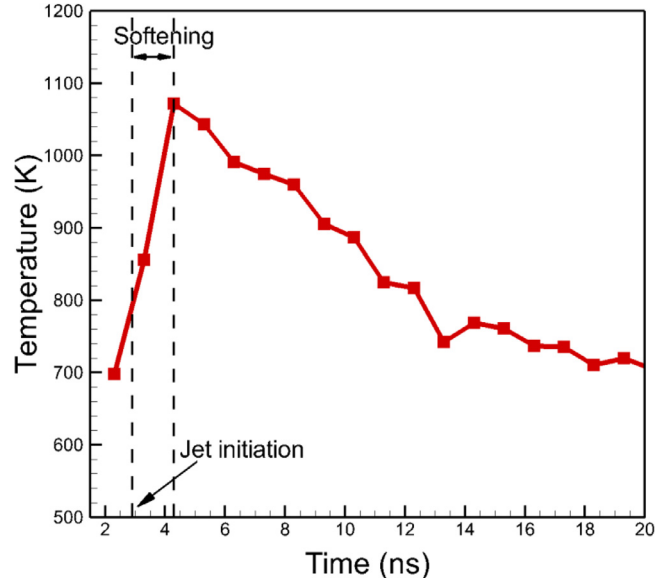


Fig. 4. The temporal evolution of the temperature at the edge of the particle/substrate interface during single particle impact for $v_i = 1300 \text{ m/s}$.

softening results in the breakdown of flow stress of the metal. A QCGD simulation is therefore also carried out to model the impact of a $25 \mu\text{m}$ liquid Al particle onto a rigid Al substrate using the same level of coarsening (L512) (see Supplementary note S3) to corroborate these results. The substrate here was kept rigid or non-compliant to observe the deformation and jetting behavior

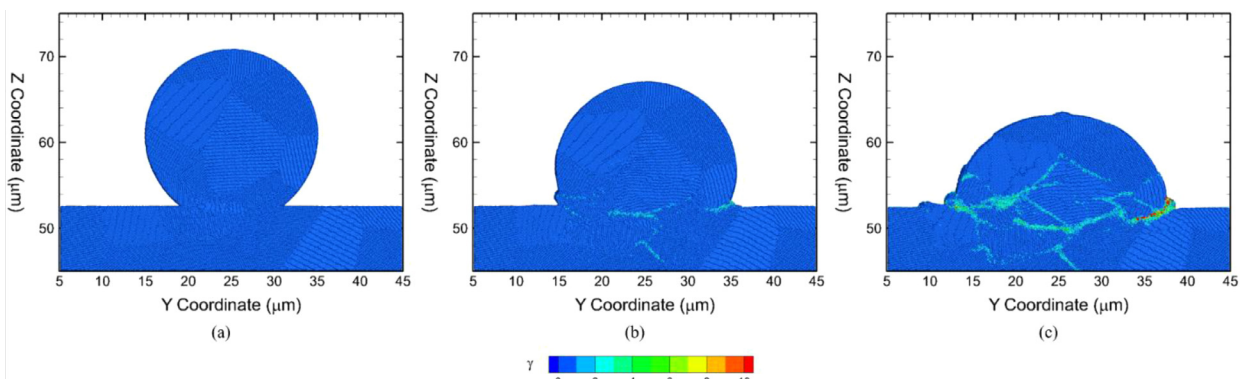


Fig. 5. Shear strain evolution for the case of $v_i = 1300 \text{ m/s}$ and $T_p \sim 165 \text{ K}$ at: (a) 1.3 ns, (b) 4.3 ns, and (c) 9.3 ns (after impact).

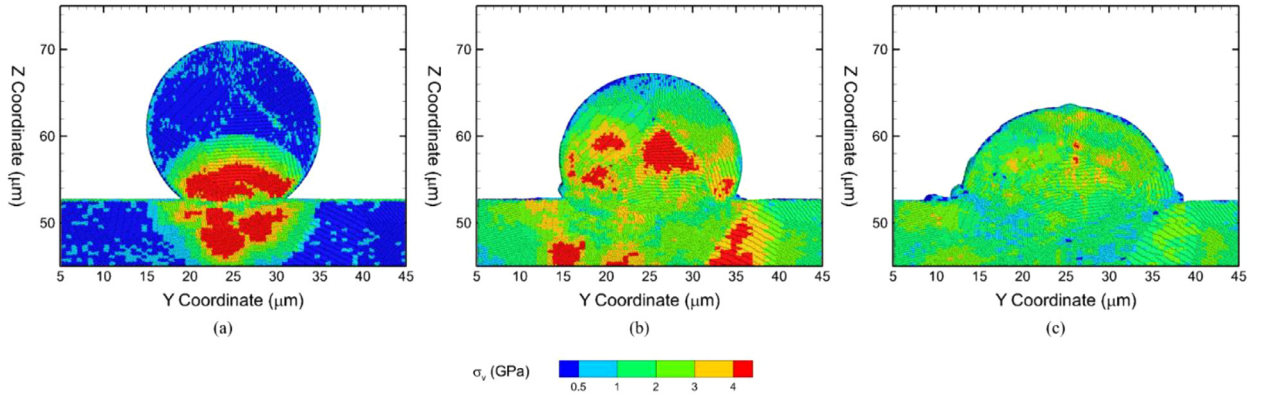


Fig. 6. von Mises stress evolution for the case of $v_i = 1300 \text{ m/s}$ and $T_p \sim 165 \text{ K}$ at times (a) 1.3 ns, (b) 4.3 ns, and (c) 9.3 ns (after impact).

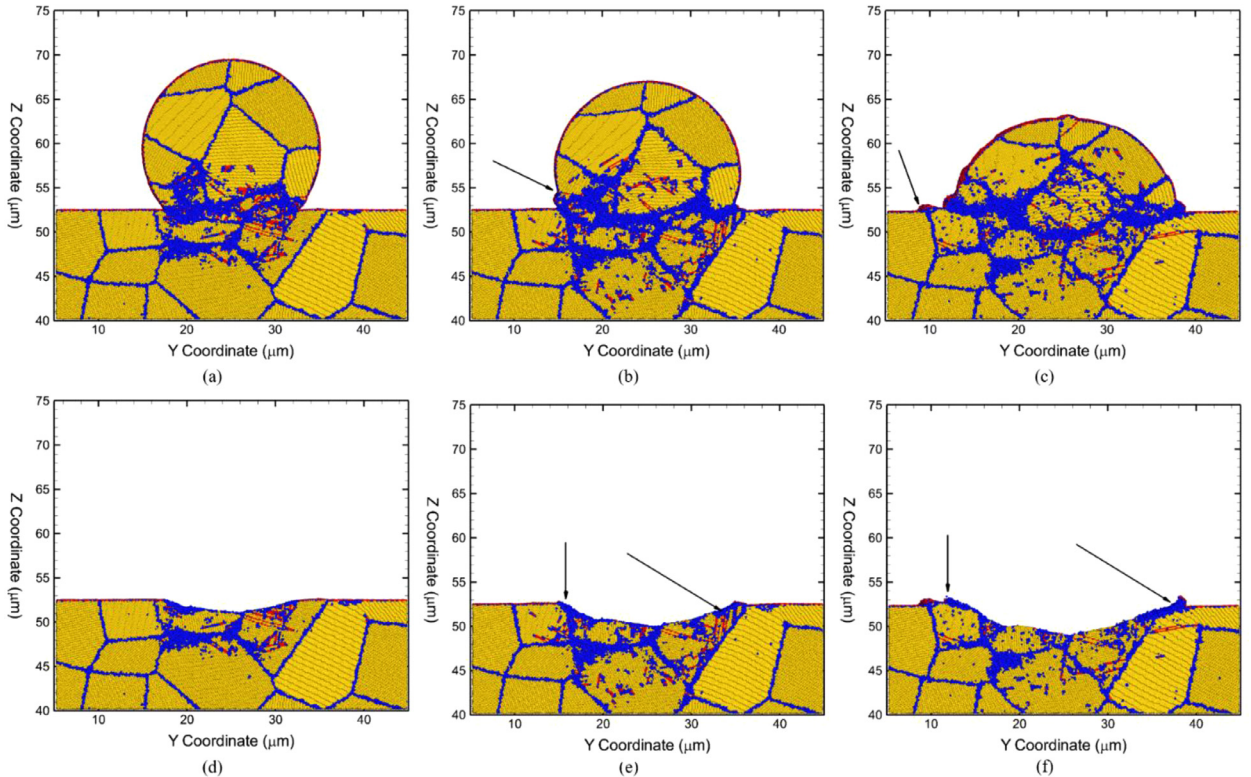


Fig. 7. Snapshots showing the microstructure of the particle (a-c) and substrate (d-e) at times of: (a, d) 2.3 ns, (b, e) 4.3 ns and (c, f) 10.3 ns (after impact) for an impact velocity of 1300 m/s. The R-atoms are colored according to the local atomic environments: fcc (yellow), hcp (red), magenta (surface) and blue (disordered). The arrows indicate the formation of a jet at the edge associated with upward flow of atoms from the substrate. Significant planar defects (twins/stacking faults – red atoms) are formed during impact (a-d) and slowly vanish as time progresses (c,f). (For interpretation of the references to colour in this figure legend, the reader is referred to the web version of this article.)

of only the particle. The impact, as shown in Figure S3, generates a shock wave that travels into the particle. The interaction of the shock wave with the particle as shown in Figure S3(b) results in the initiation of a jet at the particle/substrate interface as shown in Figure S3(c). Thus, the QCGD simulations with the same scaling relationships for coarsening show that the jetting mechanism during impact of a liquid droplet is driven by the pressure wave interaction with the particle/substrate edge as the shock velocity exceeds the edge velocity. This interaction leads to outward flow of the liquid metal leading to jet initiation at $\sim t = 1.2 \text{ ns}$. These observations suggest that the initiation of jetting behavior will be absent in particle impacts wherein the shock pressure wave is not able to interact with the interface periphery.

Although the role of the pressure wave interactions in jet initiation is clearly substantial, other variable trends like tempera-

tures and shear strains and flow stresses (von Mises) should be accounted for to obtain a complete picture of this behavior. The progressive evolution of temperatures for a single particle impact of 1300 m/s are shown in Fig. 3. The impact generates high temperatures at the interface in the region of impact as shown in Fig. 3(a). Continued deformation of the particle and substrate results in a transition in peak temperatures at the edge of the particle/substrate interface at a time of $\sim 5 \text{ ns}$ as shown in Fig. 3(b). The temperatures in these edge regions are observed to $\sim 1000 \text{ K}$, which is close to, but below, the melting temperature predicted by the interatomic potential for Al. The formation and localization of these high temperature zones allows for easier material flow at the edge of the particle/substrate interface. The temporal evolution of the temperature at the edge of the particle/substrate interface during single particle impact for $v_i = 1300 \text{ m/s}$ is shown in Fig. 4.

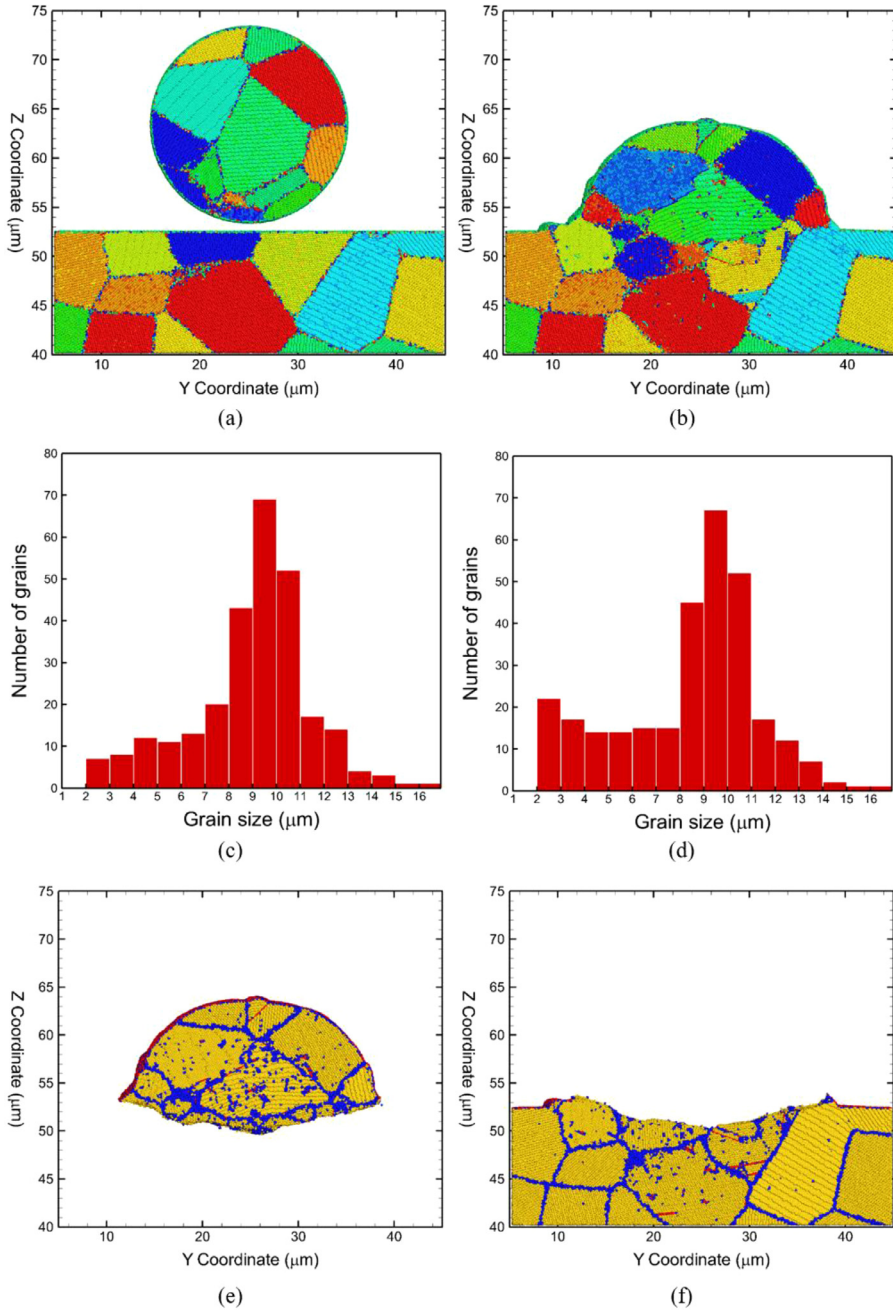


Fig. 8. Microstructural snapshots showing grain orientation representations (a, b) and grain size distributions (c, d) for a cold spray impact at $v_i = 1300 \text{ m/s}$ and $T_p \sim 165 \text{ K}$. (a, c) represent the situation before impact, and (b, d) are for $t \sim 50 \text{ ns}$ (after impact). The microstructures of the splat and substrate separately at $t = 50 \text{ ns}$ color-coded using the scheme shown in Fig. 9 are presented in (e) and (f), respectively. Grain sharing between the particle and substrate at the interface is seen here.

The plot indicates that while values as high as the melting temperature may arise, resulting in significant material softening, the temperature drops very rapidly (after $t = 4.3 \text{ ns}$, within 2 ns of jet initiation) as the material continues to flow outward. This spike in temperature is a consequence of the arrival of the plastic wave at the edge of the particle/substrate interface and the release waves result in the outward material flow and the drop in temperature at the edge.

The flow behavior of the particle/substrate at the interface can also be investigated based on the evolution of shear strains (atomic) [50,51] in the system as plotted for various times in Fig. 5. The shear strains are initially zero as shown in Fig. 5(a). Impact-induced deformation of the particle and substrate results in increased strains in the region of the impact and at the edge of

the interface as shown for a time of 4.3 ns (peak temperature and observation of a jet) in Fig. 5(b). The continued deformation of the particle results in high strains across several grain boundaries and significantly higher localized strains at the edge of the interface as shown in Fig. 5(c) for a time of 9.3 ns. Thus, large values of strain are observed well after the formation of a jet, and this is characteristic of the significant shear motion attributed to the outward flow of atoms at the particle/substrate interface. The corresponding evolution of flow stress (von Mises) is also plotted for various times in Fig. 6. The evolution of von Mises stress also drops in the regions close to the periphery edge, rises radially to the center of the interface, and drops after reaching a maximum as shown in Fig. 6(b) and (c). Similar evolution of temperature, strains and flow stress are plotted in Supplementary Figure S4

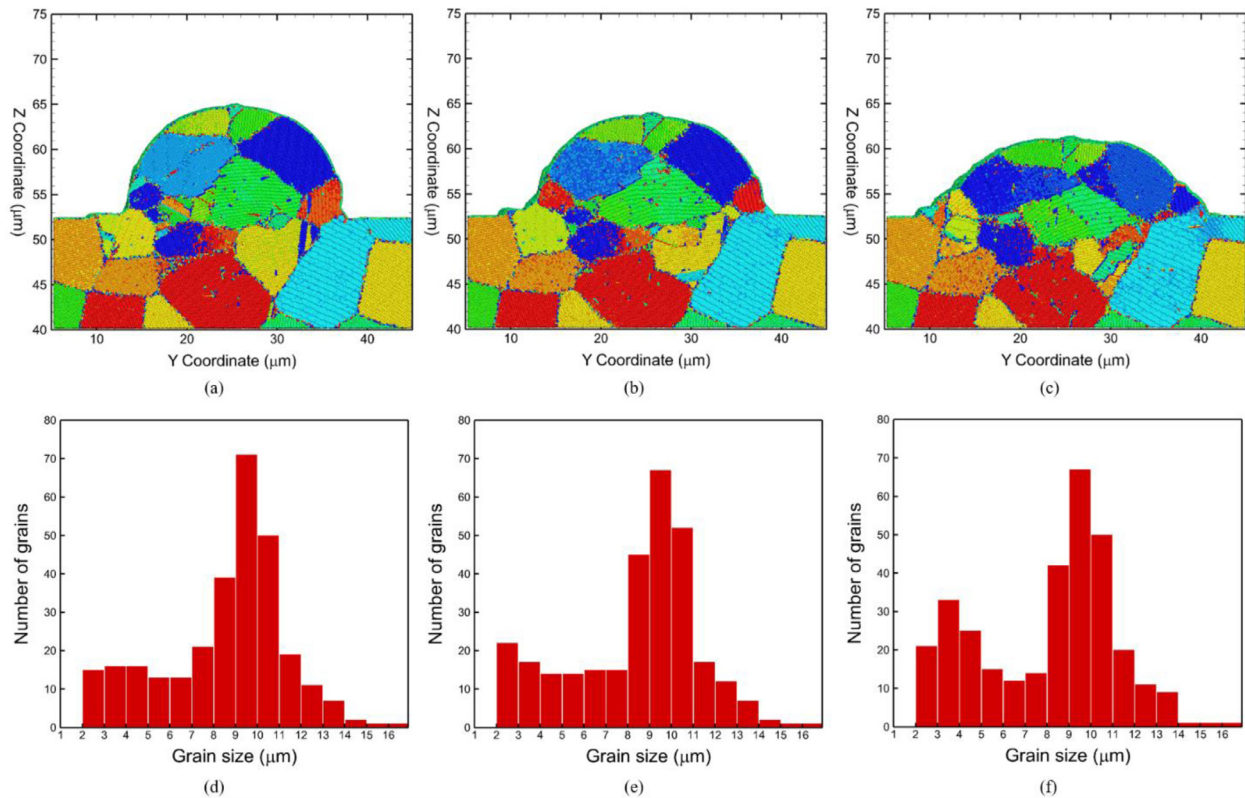


Fig. 9. Microstructural snapshots showing a grain orientation representation of a cold spray splat (a–c) and the corresponding grain size distributions (d–f) for $T_p \sim 165\text{ K}$ cold spray impact at $t \sim 50\text{ ns}$ for: (a, d) $v_i = 1100\text{ m/s}$, (b, e) $v_i = 1300\text{ m/s}$, and (c, f) $v_i = 1600\text{ m/s}$.

for the impact with a velocity of 700 m/s, where no material jetting is observed. The temperatures here are not localized at the periphery, and high shear strains are observed to be concentrated in the center of the impact region along the interface.

Leading from the comparison of evolutions of thermomechanical variables (pressures, temperatures, stresses and strains) for the cases with jetting and no jetting, it is evident that severe plastic deformation due to pressure wave propagation, interaction with the interface and its release result in localized softening of the metal at the edge, which helps to initiate the formation of a jet. Similar correlations in the evolution of temperature and strains with jetting are observed for the liquid particle impact simulation discussed above, as shown in Supplemental Figures S3(d–i). Hence, we concur with the recent work of Hassani-Gangaraj et al. [27], which identified the significant role of pressure wave interactions with the edge in initiating jetting and that this is accompanied by an increase in strains as the jet forms attributed to outward flow of material. However, the QCGD simulations do not predict a thermal boost-up zone at the edge at the suggested time scales ($\sim 30\text{ ns}$) for metal particles (Al) using FEM simulations [14,29]. For a 20 μm particle impact at 1300 m/s, the jet is observed to initiate at $\sim 2.9\text{ ns}$ which is significantly smaller than that proposed for ASI. While the observed localized softening at the edge may be considered as the thermal boost needed for jet formation, the FEM simulations do not report any decrease in temperatures due to the release of the pressures.

4. Microstructure evolution and recrystallization

Fig. 7(a)–(c) shows the microstructural snapshots corresponding to the full splat section at various times, for an impact velocity of 1300 m/s. The atoms are colored based on common neighbor analysis (CNA) method [52]: yellow atoms represent fcc stacking,

red atoms represent hcp stacking, magenta atoms represent a surface, and blue atoms represent a disordered structure. The corresponding snapshots showing only the substrate portions of the R-atoms are shown in Fig. 7(d)–(f). It can be seen that the formation of a jet at the edge is also associated with upward flow of atoms from the substrate as indicated by the arrows. An additional simulation for the same impact velocity was carried out to investigate the role of substrate microstructure (single crystal substrate). The differences in microstructural evolution in comparison with a polycrystalline substrate are discussed in detail in the Supplementary material (Note S4).

The splat microstructures are also characterized using an atom orientation clustering analysis method [53] that uses Euler orientation angles and clusters atoms with similar angles together to characterize individual grains before and after the impact. Although the temperatures generated at the interface for all 1300 m/s cases are more than $0.7T_m$ (melting temperature of aluminum as given by the EAM potential used $\sim 1050\text{ K}$), most of the particle is still at a much lower temperature, hinting that recovery is more likely than recrystallization. However, a quick comparison of the initial and final splat microstructures at a time of 50 ns showing grain orientations, as shown in Fig. 8(a) and (b), shows the formation of small grains near the interface, consolidating the possibility of recrystallization. The initial microstructure had a total of 275 grains, with an average grain size of $8.9\mu\text{m}$, and new grains are observed to form after impact of the particle when the system is allowed to evolve for 50 ns. The splat microstructure at 50 ns shows 301 grains, an increase of 26 from the microstructure before impact; there is a corresponding small reduction in the average grain size to $8.3\mu\text{m}$. The histogram analysis in Fig. 8(c) shows an increase in the number of small grains ($2\text{--}4\mu\text{m}$) in the splat microstructure at 50 ns. As expected, all the “new” grains formed are in the region close to the interface. While it is hard

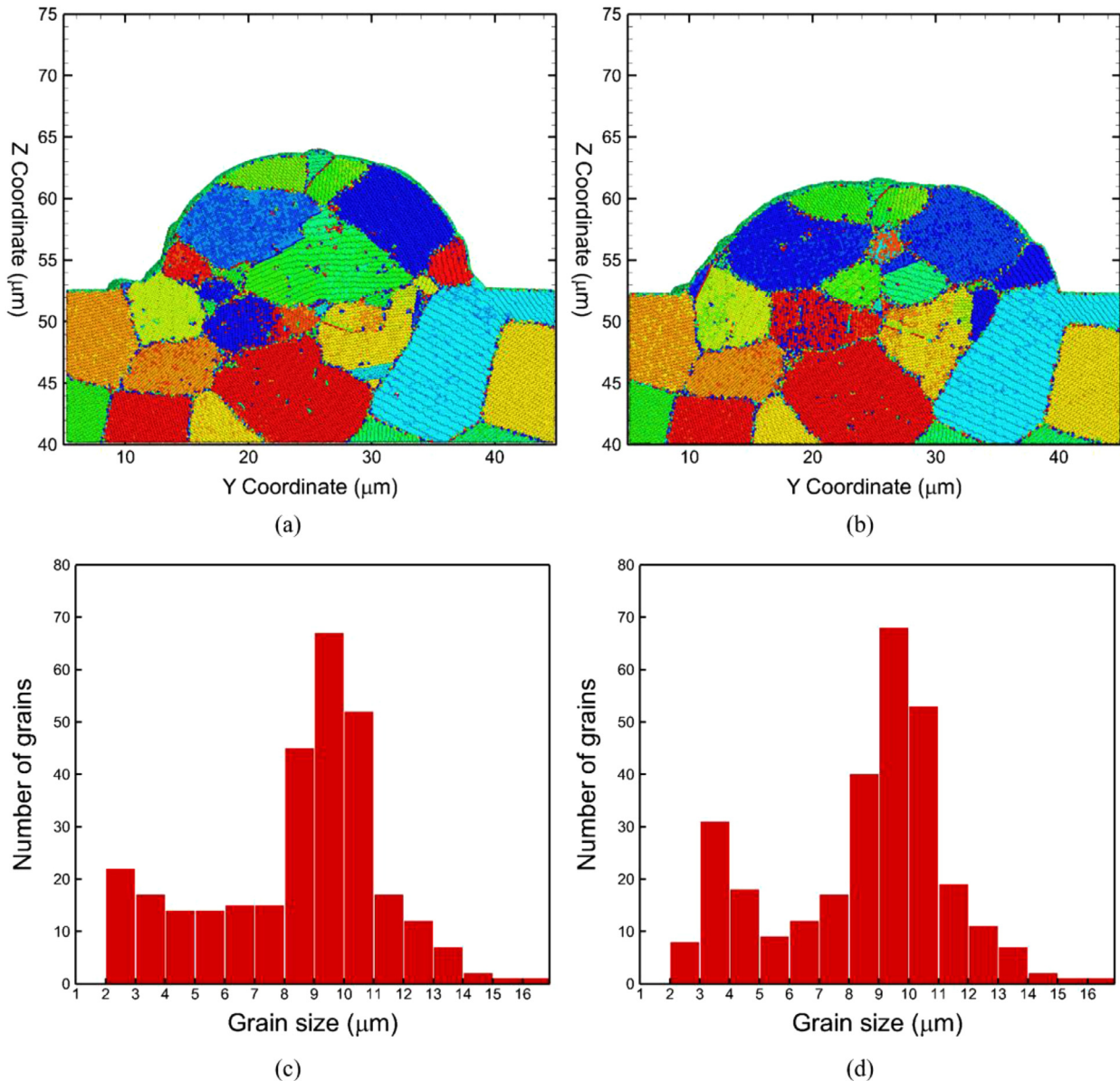


Fig. 10. Microstructural snapshots showing a grain orientation representation of a cold spray splat (a, b) and the corresponding grain size distributions (c, d) for $v_i = 1300\text{ m/s}$ cold spray impact at $t \sim 50\text{ ns}$ for: (a, c) $T_p \sim 165\text{ K}$, and (b) $T_p \sim 530\text{ K}$.

to pinpoint the specific recrystallization mechanisms [54,55] that are in play in the QCGD predicted microstructures, considering the severe deformation experienced by the system at the interface, stress induced grain boundary migration [56] may also play a key role in addition to recrystallization in the formation of new grains. For simplicity, this formation of new grains is referred to as recrystallization in this manuscript.

The evolution of microstructure and recrystallization behavior is also investigated by running the CS single particle impact simulations for particle temperatures of $\sim 165\text{ K}$, $\sim 335\text{ K}$ and $\sim 530\text{ K}$ as well as for a range of velocities, 700 m/s to 1600 m/s . The possibility of recrystallization is observed to vary with impact velocity as seen in the cold spray splats generated at a time of 50 ns showing grain orientations for $T_p \sim 165\text{ K}$ in Fig. 9. An impact velocity of 1100 m/s yields fewer recrystallized grains (20), as shown in Fig. 9(d), as compared to those observed for a higher impact velocity of 1600 m/s (47) as shown in Fig. 9(f). The increase in the number of new grains for the case of $v_i = 1600\text{ m/s}$ can be correlated to the dependence of recrystallization behavior on the strain energy

stored in the system as dislocations. Higher particle impact velocities result in more plastic deformation of the metal, and hence in generation of higher temperatures at the particle/substrate interface throughout the duration of impact. The formation of higher temperatures also promotes grain coarsening, which is observed from an increase in the grain sizes ranging from $3\text{--}4\text{ }\mu\text{m}$ and $4\text{--}5\text{ }\mu\text{m}$, as shown in Fig. 9(f). The effect of particle temperature for the same impact velocity of 1300 m/s did not show significant variation in the number of new grains formed. A comparison of the cold spray splats generated at a time of 50 ns showing grain orientations for $T_p \sim 165\text{ K}$ and $T_p \sim 530\text{ K}$ is shown in Fig. 10. For a particle temperature of $\sim 530\text{ K}$, the number of grains increased from 274 in the initial microstructure to 297 in the final microstructure as shown in Fig. 10(d). This increase is comparable to the new grains formed in the case of $T_p \sim 165\text{ K}$ as shown in Fig. 10(c). The major highlight here is the size distribution of the new grains, which lie more in the $3\text{--}4\text{ }\mu\text{m}$ and $4\text{--}5\text{ }\mu\text{m}$ regime, signifying the effect of higher particle temperatures leading to grain coarsening. A similar consensus on recrystallization behavior has been reached

in some experimental cold spray works [57–60]. It should also be noted that the embedded atom potential [47] used in this work has previously demonstrated recrystallization behavior for uniaxial loading of aluminum [61], showcasing its ability to accurately capture this phenomenon. Interestingly, some of these recrystallized grains at the interface are shared between the particle and the substrate as observed in Fig. 8(e) and (f). These results indicate that recrystallization can support the formation of a metallurgical bond between the particle and the substrate in certain areas of the interface. The experimental scenario, however, could be slightly different in the presence of a native thin oxide layer, parts of which may remain embedded at the interface centerline after impact. Further in-depth analyses of the splats in terms of characteristics like peak interfacial temperatures, compression ratio, penetration depth, interface area etc. for the above-mentioned range of particle temperatures and velocities is presented in Note S6 in the Supplementary material.

5. Conclusions and outlook

Cold spray impacts of pure aluminum powders on pure aluminum substrates are modeled using the QCGD framework for differing microstructures, particle temperatures and impact velocities. The post impact behavior is observed critically by tracking the evolution of thermomechanical variables like pressure, temperature, strain, and microstructural features like grains at the mesoscale. In particular, we investigated the role of the compressive shock wave propagation on the initiation of a jet at the particle substrate interface on the initiation of a jet at the particle substrate interface.

The simulation results indicate that the jetting behavior is attributed to the interplay between the shock wave velocity along the particle/substrate interface and the velocity of the particle/substrate interface periphery (edge) as the particle/substrate continues to deform during impact. The initiation of a jet is only observed when the shock wave velocity along the particle/substrate interface exceeds the velocity of the edge during impact. In contrast, jetting behavior is absent in particle impacts for which the shock pressure wave is not able to interact with the edge. The QCGD simulations therefore suggest that severe plastic deformation due to pressure wave propagation results in localized softening of the metal at the edge, and that the pressure release waves help to initiate the formation of a jet. This initiation of the jet is accompanied by an increase in strains as the jet forms attributed to outward flow of material. However, a thermal boost-up zone is not observed at the periphery at the time scales reported for ASI. While a thermal spike is observed following jet initiation at ~ 5 ns, it is soon followed by a gradual drop that is correlated to the release of pressure at the edge. For a 20 μm particle impact at 1300 m/s onto a pure Al substrate, the timeline of localized thermal softening and jet initiation observed in the simulations reported here is a ~ 5 ns, which is in contrast to previous reports where jet formation was attributed to ASI and several tens of nanoseconds were required.

A comparison of the initial and final splat microstructures reveals the formation of “new” small grains near the interface, which is accredited to a combination of stress driven grain boundary mobility and recrystallization mechanisms occurring at the particle/substrate interface. Some of these grains are formed at the bond line, promoting intimate contact and enhancing the bonding of the CS splat. As expected, recrystallization behavior varies with the stored strain energy and the thermal evolution in the system, with faster impacts leading to more recrystallized grains, and indications of grain coarsening at higher impact velocities as well as at higher particle temperatures. These results augment our understanding about the strengthening mechanisms in cold sprayed deposits from a modeling context. The nucleation of finer grains at

the interface and the associated grain-boundary strengthening further qualifies CS as a tunable manufacturing process in terms of achieving a desired strength of a coating.

The insights provided by these QCGD simulations represent the first *atomistic-like* approach to explore the length and timescales corresponding to practical cold spray processes. Such an approach is necessary to enhance the understanding derived from continuum-level simulations, to simulate realistic microstructures without sacrificing the effect of substrate jetting, and to predict the long-term microstructural evolution of these systems. The presence of atomic-scale impurities like oxides, alloying phases and porosity could add interesting dimensions to the interfacial behavior and will be explored in a future effort.

Declaration of Competing Interest

The authors declare that they have no known competing financial interests or personal relationships that could have appeared to influence the work reported in this paper.

Acknowledgments

This research was supported by the U.S. Army Research Laboratory under contract W911NF-15-2-0024, titled “Intelligent Processing of Materials by Design”. The authors also thank Prof. Christopher Schuh for his suggestions and discussions on the results.

Supplementary materials

Supplementary material associated with this article can be found, in the online version, at doi:[10.1016/j.actamat.2019.10.039](https://doi.org/10.1016/j.actamat.2019.10.039).

References

- [1] J. Villafuerte, Modern Cold Spray: Materials, Process, and Applications, Springer International Publishing, 2015.
- [2] V.K. Champagne, D.J. Helfritch, Mainstreaming cold spray – push for applications, *Surf. Eng.* 30 (6) (2014) 396–403.
- [3] P. Cavalieri, Cold-Spray Coatings: Recent Trends and Future Perspectives, Springer International Publishing 2017.
- [4] V.K. Champagne, The Cold Spray Materials Deposition Process: Fundamentals and Applications, Woodhead Publishing Limited, 2007.
- [5] V. Champagne, D. Helfritch, The unique abilities of cold spray deposition, *Int. Mater. Rev.* 61 (7) (2016) 437–455.
- [6] F. Gärtnér, T. Stoltenhoff, T. Schmidt, H. Kreye, The cold spray process and its potential for industrial applications, *J. Therm. Spray Technol.* 15 (2) (2006) 223–232.
- [7] M. Kamaraj, V.M. Radhakrishnan, Cold spray coating diagram: bonding properties and construction methodology, *J. Therm. Spray Technol.* 28 (4) (2019) 756–768.
- [8] X. Wang, F. Feng, M.A. Klecka, M.D. Mordasky, J.K. Garofano, T. El-Wardany, A. Nardi, V.K. Champagne, Characterization and modeling of the bonding process in cold spray additive manufacturing, *Addit. Manuf.* 8 (2015) 149–162.
- [9] T. Stoltenhoff, H. Kreye, H.J. Richter, An analysis of the cold spray process and its coatings, *Journal of Thermal Spray Technology* 11 (4) (2002) 542–550.
- [10] A.C. Hall, L.N. Brewer, T.J. Roemer, Preparation of aluminum coatings containing homogenous nanocrystalline microstructures using the cold spray process, *J. Therm. Spray Technol.* 17 (3) (2008) 352–359.
- [11] L. Ajdelsztajn, J.M. Schoenung, B. Jodoin, G.E. Kim, Cold spray deposition of nanocrystalline aluminum alloys, *Metall. Mater. Trans. A* 36 (3) (2005) 657–666.
- [12] B.A. Bedard, T.J. Flanagan, A.T. Ernst, A. Nardi, A.M. Dongare, H.D. Brody, V.K. Champagne, S.-W. Lee, M. Aindow, Microstructure and micromechanical response in gas-atomized al 6061 alloy powder and cold-sprayed splats, *J. Therm. Spray Technol.* 27 (8) (2018) 1563–1578.
- [13] H. Koivuluoto, G. Boellini, L. Lusvarghi, F. Casadei, P. Vuoristo, Corrosion resistance of cold-sprayed Ta coatings in very aggressive conditions, *Surf. Coat. Technol.* 205 (4) (2010) 1103–1107.
- [14] G. Bae, Y. Xiong, S. Kumar, K. Kang, C. Lee, General aspects of interface bonding in kinetic sprayed coatings, *Acta Mater.* 56 (17) (2008) 4858–4868.
- [15] W. Xie, A. Alizadeh-Dehkhangani, Q. Chen, V.K. Champagne, X. Wang, A.T. Nardi, S. Kooi, S. Müftü, J.-H. Lee, Dynamics and extreme plasticity of metallic microparticles in supersonic collisions, *Sci. Rep.* 7 (1) (2017) 5073.
- [16] M. Hassani-Gangaraj, D. Veysset, K.A. Nelson, C.A. Schuh, In-situ observations of single micro-particle impact bonding, *Scr. Mater.* 145 (2018) 9–13.

- [17] M. Hassani-Gangaraj, D. Veysset, K.A. Nelson, C.A. Schuh, Impact-bonding with aluminum, silver, and gold microparticles: toward understanding the role of native oxide layer, *Appl. Surf. Sci.* 476 (2019) 528–532.
- [18] Y. Xie, S. Yin, C. Chen, M.-P. Planche, H. Liao, R. Lupoi, New insights into the coating/substrate interfacial bonding mechanism in cold spray, *Scr. Mater.* 125 (2016) 1–4.
- [19] M. Fukumoto, M. Mashiko, M. Yamada, E. Yamaguchi, Deposition behavior of copper fine particles onto flat substrate surface in cold spraying, *J. Therm. Spray Technol.* 19 (1) (2010) 89–94.
- [20] W.-Y. Li, C.-J. Li, H. Liao, Significant influence of particle surface oxidation on deposition efficiency, interface microstructure and adhesive strength of cold-sprayed copper coatings, *Appl. Surf. Sci.* 256 (16) (2010) 4953–4958.
- [21] R.L. Maev, A. Papyrin, Structure formation of ni-based composite coatings during low pressure gas dynamic spraying, in: Proceedings of the 2006 ITSC, Seattle, WA, ASM, 2006.
- [22] T. Hussain, D.G. McCartney, P.H. Shipway, D. Zhang, Bonding mechanisms in cold spraying: the contributions of metallurgical and mechanical components, *J. Therm. Spray Technol.* 18 (3) (2009) 364–379.
- [23] Q. Wang, N. Birbilis, M.-X. Zhang, Interfacial structure between particles in an aluminum deposit produced by cold spray, *Mater. Lett.* 65 (11) (2011) 1576–1578.
- [24] V.K. Champagne, D. Helfritch, P. Leyman, S. Grendahl, B. Klotz, Interface material mixing formed by the deposition of copper on aluminum by means of the cold spray process, *J. Therm. Spray Technol.* 14 (3) (2005) 330–334.
- [25] S. Guetta, M.H. Berger, F. Borit, V. Guiport, M. Jeandin, M. Boustie, Y. Ichikawa, K. Sakaguchi, K. Ogawa, Influence of particle velocity on adhesion of cold-sprayed splats, *J. Therm. Spray Technol.* 18 (3) (2009) 331–342.
- [26] G. Bae, S. Kumar, S. Yoon, K. Kang, H. Na, H.-J. Kim, C. Lee, Bonding features and associated mechanisms in kinetic sprayed titanium coatings, *Acta Mater.* 57 (19) (2009) 5654–5666.
- [27] M. Hassani-Gangaraj, D. Veysset, V.K. Champagne, K.A. Nelson, C.A. Schuh, Adiabatic shear instability is not necessary for adhesion in cold spray, *Acta Mater.* 158 (2018) 430–439.
- [28] J. Vlcek, L. Gimeno, H. Huber, E. Lugscheider, A systematic approach to material eligibility for the cold-spray process, *J. Therm. Spray Technol.* 14 (1) (2005) 125–133.
- [29] H. Assadi, F. Gärtner, T. Stoltenhoff, H. Kreye, Bonding mechanism in cold gas spraying, *Acta Mater.* 51 (15) (2003) 4379–4394.
- [30] M. Grujicic, C.L. Zhao, W.S. DeRosset, D. Helfritch, Adiabatic shear instability based mechanism for particles/substrate bonding in the cold-gas dynamic-spray process, *Mater. Des.* 25 (8) (2004) 681–688.
- [31] M. Yu, W.-Y. Li, F.F. Wang, H.L. Liao, Finite element simulation of impacting behavior of particles in cold spraying by Eulerian approach, *Journal of Thermal Spray Technology* 21 (3) (2012) 745–752.
- [32] H. Assadi, F. Gärtner, T. Klassen, H. Kreye, Comment on ‘Adiabatic shear instability is not necessary for adhesion in cold spray’, *Scr. Mater.* 162 (2019) 512–514.
- [33] P. Landau, S. Osovski, A. Venkert, V. Gärtnerová, D. Rittel, The genesis of adiabatic shear bands, *Sci. Rep.* 6 (2016) 37226.
- [34] D. Rittel, P. Landau, A. Venkert, Dynamic recrystallization as a potential cause for adiabatic shear failure, *Phys. Rev. Lett.* 101 (16) (2008) 165501.
- [35] D.J. Benson, A multi-material Eulerian formulation for the efficient solution of impact and penetration problems, *Comput. Mech.* 15 (6) (1995) 558–571.
- [36] S. Yin, H.L. Liao, X.F. Wang, Euler based finite element analysis on high velocity impact behaviour in cold spraying, *Surf. Eng.* 30 (5) (2014) 309–315.
- [37] S. Rahmati, A. Ghaei, The use of particle/substrate material models in simulation of cold-gas dynamic-spray process, *J. Therm. Spray Technol.* 23 (3) (2014) 530–540.
- [38] C.M. Kay, J. Karthikeyan, High Pressure Cold Spray: Principles and Applications, ASM International, 2016.
- [39] L.E. Murr, A. Ayala, C.S. Niou, Microbands and shear-related microstructural phenomena associated with impact craters in 6061-T6 aluminum, *Mater. Sci. Eng. A* 216 (1) (1996) 69–79.
- [40] L.E. Murr, E.V. Esquivel, Observations of common microstructural issues associated with dynamic deformation phenomena: twins, microbands, grain size effects, shear bands, and dynamic recrystallization, *J. Mater. Sci.* 39 (4) (2004) 1153–1168.
- [41] A.M. Dongare, Quasi-coarse-grained dynamics: modelling of metallic materials at mesoscales, *Philos. Mag.* 94 (34) (2014) 3877–3897.
- [42] G. Agarwal, A.M. Dongare, Defect and damage evolution during spallation of single crystal Al: comparison between molecular dynamics and quasi-coarse-grained dynamics simulations, *Comput. Mater. Sci.* 145 (2018) 68–79.
- [43] G. Agarwal, R.R. Valisetty, R.R. Namburu, A.M. Rajendran, A.M. Dongare, The quasi-coarse-grained dynamics method to unravel the mesoscale evolution of defects/damage during shock loading and spall failure of polycrystalline Al microstructures, *Sci. Rep.* 7 (1) (2017) 12376.
- [44] G. Agarwal, A.M. Dongare, Modeling the thermodynamic behavior and shock response of Ti systems at the atomic scales and the mesoscales, *J. Mater. Sci.* 52 (18) (2017) 10853–10870.
- [45] S. Suresh, S.-W. Lee, M. Aindow, H.D. Brody, V.K. Champagne, A.M. Dongare, Unraveling the Mesoscale evolution of microstructure during supersonic impact of aluminum powder particles, *Sci. Rep.* 8 (1) (2018) 10075.
- [46] P.M. Derlet, H. Van Swygenhoven, Atomic positional disorder in fcc metal nanocrystalline grain boundaries, *Phys. Rev. B* 67 (1) (2003) 014202.
- [47] Y. Mishin, D. Farkas, M.J. Mehl, D.A. Papaconstantopoulos, Interatomic potentials for monoatomic metals from experimental data and ab initio calculations, *Phys. Rev. B* 59 (5) (1999) 3393–3407.
- [48] J.P. Dear, J.E. Field, High-speed photography of surface geometry effects in liquid/solid impact, *J. Appl. Phys.* 63 (4) (1988) 1015–1021.
- [49] J.E. Field, J.P. Dear, J.E. Ogren, The effects of target compliance on liquid drop impact, *J. Appl. Phys.* 65 (2) (1989) 533–540.
- [50] M.L. Falk, J.S. Langer, Dynamics of viscoplastic deformation in amorphous solids, *Phys. Rev. E* 57 (6) (1998) 7192–7205.
- [51] A. Stukowski, Visualization and analysis of atomistic simulation data with OVITO – the open visualization tool, *Modell. Simul. Mater. Sci. Eng.* 18 (1) (2009) 015012.
- [52] J.D. Honeycutt, H.C. Andersen, Molecular dynamics study of melting and freezing of small Lennard-Jones clusters, *J. Phys. Chem.* 91 (19) (1987) 4950–4963.
- [53] J. Chen, A.M. Dongare, Atom clustering analysis to detect grains and twins in metal microstructures, *Comp. Mater. Sci.* (in preparation).
- [54] M.R. Rokni, C.A. Widener, V.R. Champagne, Microstructural stability of ultra-fine grained cold sprayed 6061 aluminum alloy, *Appl. Surf. Sci.* 290 (2014) 482–489.
- [55] M.R. Rokni, A. Zarei-Hanzaki, H.R. Abedi, Microstructure evolution and mechanical properties of back extruded 7075 aluminum alloy at elevated temperatures, *Mater. Sci. Eng. A* 532 (2012) 593–600.
- [56] K. Cheng, L. Zhang, C. Lu, K. Tie, Coupled grain boundary motion in aluminium: the effect of structural multiplicity, *Sci. Rep.* 6 (2016) 25427.
- [57] Y. Zou, D. Goldbaum, J.A. Szpunar, S. Yue, Microstructure and nanohardness of cold-sprayed coatings: electron backscattered diffraction and nanoindentation studies, *Scr. Mater.* 62 (6) (2010) 395–398.
- [58] K. Yang, W. Li, X. Guo, X. Yang, Y. Xu, Characterizations and anisotropy of cold-spraying additive-manufactured copper bulk, *J. Mater. Sci. Technol.* 34 (9) (2018) 1570–1579.
- [59] M.R. Rokni, C.A. Widener, V.K. Champagne, G.A. Crawford, Microstructure and mechanical properties of cold sprayed 7075 deposition during non-isothermal annealing, *Surf. Coat. Technol.* 276 (2015) 305–315.
- [60] M.R. Rokni, C.A. Widener, G.A. Crawford, Microstructural evolution of 7075 Al gas atomized powder and high-pressure cold sprayed deposition, *Surf. Coat. Technol.* 251 (2014) 254–263.
- [61] X. Li, Y. Wei, W. Yang, H. Gao, Competing grain-boundary- and dislocation-mediated mechanisms in plastic strain recovery in nanocrystalline aluminum, *Proc. Natl. Acad. Sci.* 106 (38) (2009) 16108.